Coupled protein domain motion in Taq polymerase revealed by neutron spin-echo spectroscopy

Zimei Bu, Ralf Biehl, Michael Monkenbusch, Dieter Richter, and David J. E. Callaway

This information is current as of May 2007.

Notes:

Coupled protein domain motion in *Taq* polymerase revealed by neutron spin-echo spectroscopy

Zimei Bu*[†], Ralf Biehl[‡], Michael Monkenbusch[‡], Dieter Richter[‡], and David J. E. Callaway*[†§]

*Fox Chase Cancer Center, 333 Cottman Avenue, Reimann 414, Philadelphia, PA 19111; [‡]Institut für Festkörperforschung, Forschungszentrum Jülich, D-52425 Jülich, Germany; and [§]Department of Neurology, New York University School of Medicine, 350 Community Drive, Manhasset, NY 11030

Long-range conformational changes in proteins are ubiquitous in biology for the transmission and amplification of signals; such conformational changes can be triggered by small-amplitude, nanosecond protein domain motion. Understanding how conformational changes are initiated requires the characterization of protein domain motion on these timescales and on length scales comparable to protein dimensions. Using neutron spin-echo spectroscopy (NSE), normal mode analysis, and a statistical-mechanical framework, we reveal overdamped, coupled domain motion within DNA polymerase I from *Thermus aquaticus* (*Taq* polymerase). This protein utilizes correlated domain dynamics over 70 Å to coordinate nucleotide synthesis and cleavage during DNA synthesis and repair. We show that NSE spectroscopy can determine the domain mobility tensor, which determines the degree of dynamical coupling between domains. The mobility tensor defines the domain velocity response to a force applied to it or to another domain, just as the sails of a sailboat determine its velocity given the applied wind force. The NSE results provide insights into the nature of protein domain motion that are not appreciated by conventional biophysical techniques.

normal mode analysis | statistical mechanics | protein dynamics | quasielastic neutron scattering

Protein domain motions are critical for proteins to coordinate precise biological functions. For example, coupled domain motions occur in genome regulatory proteins, motor proteins, signaling proteins, and structural proteins (1–6). Structural studies have documented the conformational flexibility in proteins accompanying their activities (7). Results from macroscopic studies, such as biochemical kinetics and single molecule detection studies, have also shown the importance of conformational dynamics and Brownian thermal fluctuations within proteins (5, 8–10). However, the time-dependent, dynamic processes that facilitate protein domain rearrangements remain poorly understood.

The function of DNA polymerase I from *Thermus aquaticus* (*Taq* polymerase) (see Fig. 1) requires coordinated domain and subdomain motions within this protein to generate a precise ligatable nick on a DNA duplex (11–13). *Taq* polymerase performs nucleotide replacement reactions in DNA repair and RNA primer removal in DNA replication (14). During such processes, *Taq* polymerase utilizes a DNA polymerase domain to catalyze the addition of dNTP to the 3′ hydroxyl terminus of an RNA primer and a 5′ nuclease domain to cleave the downstream, single-stranded 5′ nucleotide displaced by the growing upstream strand (11). Because the structure of *Taq* polymerase possesses an extended conformation with the polymerase and the 5′ nuclease active sites separated by ≈70 Å (15–17), the DNA needs to be shuttled between these two distant catalytic sites when switching from the DNA synthesis mode to the nucleotide cleavage mode. This scenario is similar to that which occurs when the DNA needs to be shifted from the polymerase active site to the 3′–5′ exonuclease catalytic center, which are ≈30 Å apart in the Klenow fragment (the polymerase domain plus the 3′–5′ exonuclease domain) domain of polymerase I, to cleave an

incorrectly incorporated dNTP (18). In addition, the polymerase domain can communicate with the 5′ nuclease domain, as evidenced by biochemical experiments that show that the presence of the polymerase domain affects the activity of the 5′ nuclease domain (12, 19). These studies imply that dynamic coupling among protein domains plays a very significant (if not well appreciated) role in their biological functions.

We have studied protein domain motions in *Taq* polymerase by neutron spin-echo spectroscopy (NSE). NSE is a quasielastic neutron scattering (QENS) technique that can study long-range relaxation processes in a macromolecule on timescales up to 100 ns and on length scales from 5 to 150 Å (20, 21). Conventional QENS techniques (e.g., time-of-flight and back-scattering) have been used to study the incoherent dynamics of hydrogen atoms within proteins on $0.1 \le Q \le 2$ Å^{-1} (where $Q = 4\pi\sin\theta/\lambda$ is the magnitude of the scattering vector, with 2θ being the scattering angle and λ the wavelength of the neutrons) and on timescales of 10^{-12} to 10^{-10} s (22–26). For a protein in D$_2$O buffer solution, NSE mainly measures coherent scattering in the Q region of $0.02 \le Q \le 0.3$ Å^{-1} (in this study), as in small-angle neutron scattering (SANS). However, rather than the static correlation function obtained by SANS, NSE gives information about the time evolution of the correlation function. NSE is analogous to dynamic light scattering (DLS), but the timescales and length scales are better suited for the mesoscopic scale of the internal modes of macromolecules than DLS. Here, we show that NSE can resolve the domain mobility tensor of a protein, thus specifying how protein domains are dynamically coupled during global conformational changes.

Methods

NSE Experiments. The expression and purification of *Taq* polymerase have been described in ref. 17. Before NSE experiments, *Taq* polymerase was exchanged into 99.9% D$_2$O buffer containing 25 mM per-deuterated Tris-d$_{11}$ (Cambridge Isotope Laboratories, Cambridge, MA) (pH^2 8.0) and 75 mM NaCl repeatedly by using a Centriprep concentrator (Millipore). The protein concentration used for NSE experiment was ≈8 mg/ml in D$_2$O solution. This protein concentration is dilute to eliminate intermolecular interaction effects (17).

NSE experiments were conducted at the Institut für Festkörperforschung (27). The wavelength was 8.6 Å. The path length of the sample cell was 4 mm. The data were collected over the range of 0.039 Å^{-1} ≤ Q ≤ 0.260 Å^{-1}. NSE experiments were performed at 30°C.

The $S(Q,t)/S(Q,0)$ spectra can be approximated by the first cumulant representation as

---

Normal mode 7

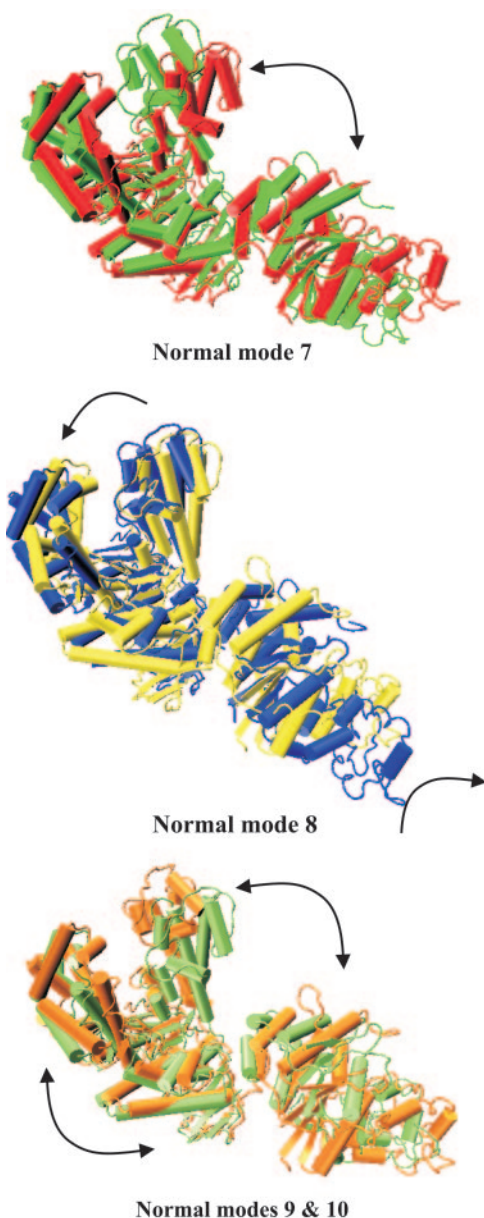**Normal mode 8**

Normal modes 9 & 10

Fig. 1. Structure of *Taq* polymerase and NMA. *Taq* polymerase has two distinct domains: a 5′ nuclease (residues 1–289) and a Klentaq (residues 294–831) connected by a linker (residues 290–305). Klentaq resembles a right hand with palm, finger, and thumb subdomains. NMA on *Taq* polymerase using ELNEMO (34) can identify the type and direction of internal motions. Klentaq can be subdivided into the 3′–5′ exonuclease domain (residues 294–422) and the polymerase domain (residues 424–831). The first six normal modes are the translational and rotational motions of *Taq* polymerase as a whole (not shown). The lowest internal seventh and eighth normal modes are relative *en bloc* motions between Klentaq and 5′ nuclease with 5′ nuclease moving toward the thumb, which is functionally important (17). Subdomain motions become apparent for the 9th, 10th, and higher normal modes.

$$\ln \frac{S(Q, t)}{S(Q, 0)} = -\bar{\Gamma}(Q)t + \frac{1}{2} K_2 t^2 - \frac{1}{3!} K_3 t^3 + \cdots, \quad \textbf{[1a]}$$

where the decay rate of the dynamic form factor is

$$\bar{\Gamma}(Q) = -\lim_{t \to 0} \frac{\partial}{\partial t} \ln[S(Q, t)], \quad \textbf{[1b]}$$
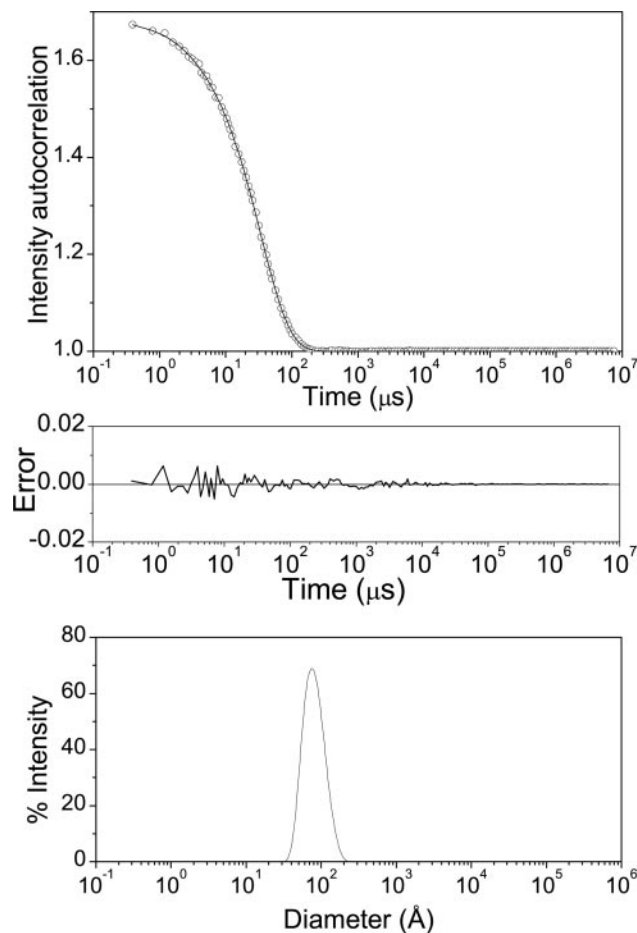
Fig. 2. Macroscopic hydrodynamic properties of *Taq* polymerase by DLS. *Top* shows the DLS-measured correlation function (○). The solid line is the regularization fit to the correlation function. *Middle* shows the sum-of-squares differences between the experimental measured autocorrelation function and the fit. *Bottom* shows Laplace transformation of the regularization fit. A single peak indicates the absence of aggregation of *Taq* polymerase. The measured center-of-mass translational diffusion coefficient is $D_{t,DLS} = (4.7 \pm 0.2) \times 10^{-7}$ cm²/s in D₂O at 30.0°C, which leads to a hydrodynamic radius $R_h = 45.9 \pm 0.2$ Å by the Stokes–Einstein equation $R_h = k_B T / 6\pi\eta D_t$.

and the effective diffusion coefficient is

$$D_{\text{eff}}(Q) = \frac{\bar{\Gamma}(Q)}{Q^2}. \quad \textbf{[1c]}$$

DLS Experiments. DLS experiments were performed with a DynaPro (Wyatt Technology, Santa Barbara, CA), using a laser of wavelength of 824.7 nm at a fixed angle of 90°, corresponding to $Q = 0.00108$ Å⁻¹. The *Taq* polymerase concentration was 0.25 mg/ml in 70 mM NaCl/35 mM Tris·HCl, pH 8.0, in which the intermolecular interaction effect is eliminated. The DLS experiments were performed at 30.0°C in D₂O buffer. Because the size of *Taq* polymerase is much smaller than the wavelength of light used in a DLS experiment ($QR_g \approx 0.04$, with R_g being the radius of gyration of *Taq* polymerase), DLS measures the center-of-mass translational diffusion constant of *Taq* polymerase. DLS experiments show that *Taq* polymerase does not aggregate in D₂O solution in which we conducted the NSE experiments (see Fig. 2).

Solution Small-Angle X-Ray Scattering (SAXS) Experiment. SAXS experiments were conducted with an in-house apparatus (28).

The effective Q range covered was from 0.016 to 0.35 Å^{-1}. The *Taq* polymerase concentration was 5 mg/ml in 70 mM NaCl/35 mM Tris·HCl, pH 8.0/H$_2$O buffer. SAXS experiments were performed at 30.0°C. SAXS data reduction and data analysis procedures have been described in ref. 28. Inverse Fourier transformation of $I(Q)$ gives the length distribution function $P(r)$, which is the probability of finding two scattering points at a given distance r from each other in the measured macromolecule. Inverse Fourier transformation of $I(Q)$ gives the length distribution function $P(r)$, which is the probability of finding two scattering points at a given distance r from each other in the measured macromolecule (29):

$$P(r) = \frac{1}{2\pi^2} \int I(Q) Qr \sin(Qr) dQ.$$

Calculating $D_{\text{eff}}(Q)$ for a Rigid-Body Model of *Taq* Polymerase. A formula derived by J. M. Schurr (personal communication) was used to calculate the first cumulant $D_{\text{eff}}(Q)$ of a rigid-body model of *Taq* polymerase from the x-ray crystal structure coordinates (Protein Data Bank ID code 1TAQ) (15):

$$D_{\text{eff}}(Q) = \frac{k_B T}{Q^2} \frac{\sum_{jl} \langle b_j b_l (QH^T Q + L(j) H^R L(l)) e^{iQ(r_j - r_l)} \rangle}{\sum_{jl} \langle b_j b_l e^{iQ(r_j - r_l)} \rangle},$$

[2]

where b_j and b_l are the neutron scattering lengths of effective residues j and l, respectively. The sum was taken over effective residues j and l, with the center of each effective residue taken as the average coordinate of the atoms in the effective residue and with the neutron scattering length b of the effective residue being the sum of neutron scattering lengths of all atoms in a residue. In Eq. **2**, $L(j) = Q \times r_j$ is the angular momentum vector, and H^T and H^R are the translational and rotational mobility tensors, respectively. The three principal-axis translational diffusion coefficients D_x^T, D_y^T, and D_z^T in H^T and the three principal-axis rotational diffusion coefficients D_x^R, D_y^R, and D_z^R in H^R were obtained from the *Taq* polymerase crystal structure coordinates (PDB ID code 1TAQ) (15) by using the program HYDROPRO, created by Garcia de la Torre and coworkers (30, 31). The integration over the two Euler angles (β, γ) of Q was performed numerically by the trapezoid rule, with step sizes of 0.01 in both $\cos\beta$ and γ proving to be adequate.

Results and Discussion

Unusual Internal Dynamic Behavior in *Taq* Polymerase Revealed by NSE. The NSE-measured dynamic form factor $S(Q, t)/S(Q, 0)$ from *Taq* polymerase can be fitted with single exponential decay functions as shown in Fig. 3*A*. However, the nonlinearity of the decay rate $\bar{\Gamma}(Q)$ of $S(Q, t)/S(Q, 0)$ as a function of Q^2 shown in Fig. 3*B* indicates that NSE has revealed a dynamic behavior in *Taq* polymerase that is significantly different from the center-of-mass diffusion of a macromolecule. The effective diffusion coefficient $D_{\text{eff}}(Q)$ oscillates, as a function of Q, around the center-of-mass translational diffusion constant measured by DLS ($D_{\text{t,DLS}}$) (see Fig. 4*A*). The oscillatory behavior of $D_{\text{eff}}(Q)$ as a function of Q indicates that NSE has detected the presence of internal dynamics in *Taq* polymerase.

We first examine the contributions of rigid-body translational and rotational diffusion to the oscillatory behavior of $D_{\text{eff}}(Q)$ because the intramolecular interference in the static form factor of a rigid structure could, in principle, cause the oscillations in D_{eff} (32, 33). The $D_{\text{eff}}(Q)$ calculated by the rigid-body model using Eq. **2** is shown in Fig. 4*A*. Although the experimental
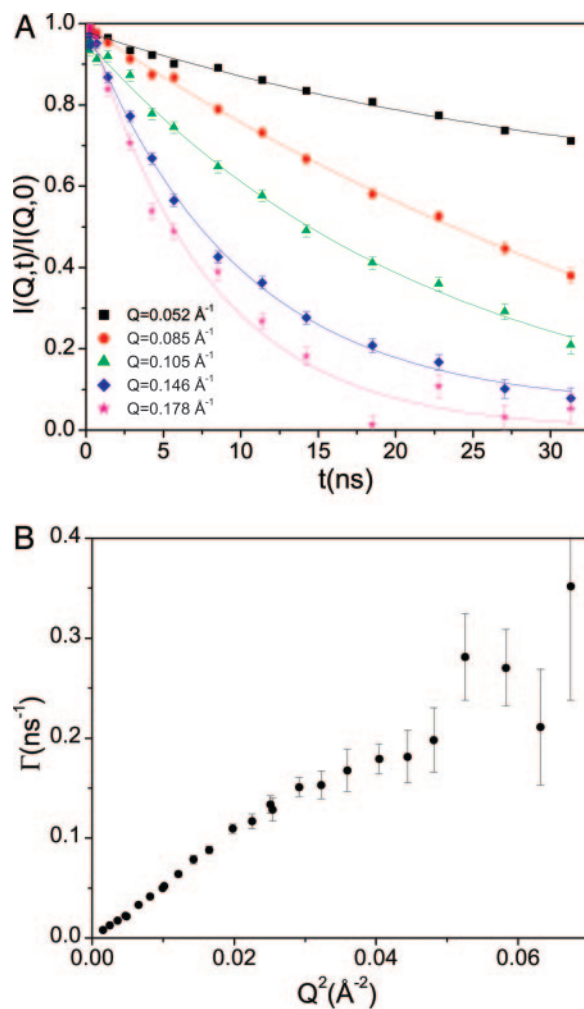

Fig. 3. NSE spectra as a function of time t at several representative Q values. (*A*) The $S(Q,t)/S(Q,0)$ spectra can be fitted with single exponential decay functions (solid lines) with $\chi^2 < 1.2$ to obtain the decay rate $\Gamma(Q)$. (*B*) The decay rate $\bar{\Gamma}(Q)$ of $S(Q,t)/S(Q,0)$ as a function of Q^2.

$D_{\text{eff}}(Q)$ has maximums and minimums (see Fig. 4*A*) that correspond to the dip and rise in $I(Q)$ (shown in Fig. 4*B*), respectively, the experimental $D_{\text{eff}}(Q)$ shows much more significant oscillations than the calculated $D_{\text{eff}}(Q)$ using Eq. **2** of the rigid-body model. Fig. 4*A* shows that the $D_{\text{eff}}(Q)$ derived from Eq. **2** only agrees with the experimental data in the region of $Q < 0.125$ Å^{-1}, suggesting that *Taq* polymerase behaves as a rigid body only on length scales longer than $2\pi/Q > 50$ Å. As $Q > 0.125$ Å^{-1}, the NSE-measured $D_{\text{eff}}(Q)$ oscillates more markedly than that calculated by Eq. **2** of the rigid-body model. Thus, the dynamic behavior of *Taq* polymerase cannot be described by the rigid-body model when $Q > 0.125$ Å^{-1}.

Next, we compare the structure of *Taq* polymerase in solution by SAXS with the crystal structure to examine whether the existence of multiple static structures in solution could possibly cause the deviations of the NSE-measured $D_{\text{eff}}(Q)$ from the rigid-body behavior. The static form factor $I(Q)$ calculated from the crystal structure coordinates is shown in Fig. 4*B*, together with that measured by solution SAXS, which is an ensemble average of all possible structures that can be adopted by *Taq* polymerase in solution. The length distribution functions $P(r)$ calculated from the crystal structure and solution SAXS data are also plotted in Fig. 4*C*. As shown in Fig. 4 *B* and *C*, both $I(Q)$ and $P(r)$ from solution SAXS are very similar to those calculated
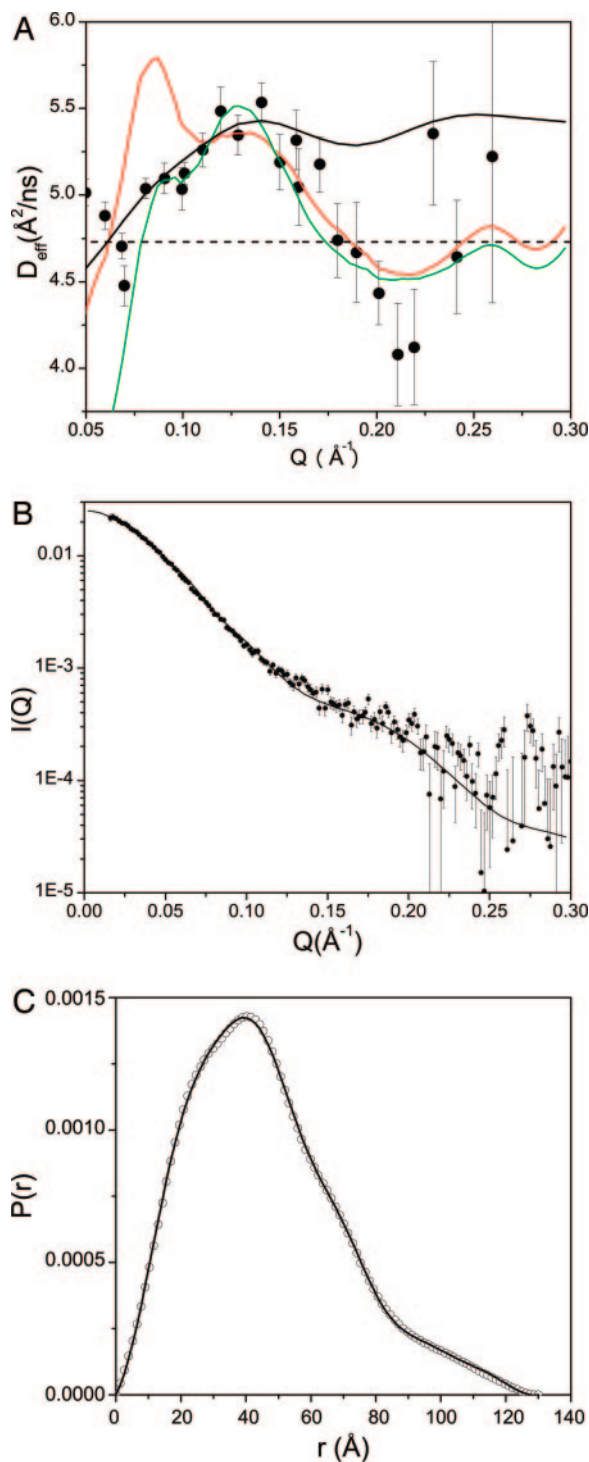
Fig. 4. NSE reveals internal motion within *Taq* polymerase. (*A*) Comparing the experimental $D_{eff}(Q) = \bar{\Gamma}(Q)/Q^2$ of *Taq* polymerase by NSE (●) with those from different dynamic models. The horizontal dashed line is $D_{t,DLS}$. The black solid line is the $D_{eff}(Q)$ of a rigid-body model of *Taq* polymerase calculated by Eq. **2**. The red line is the $D_{eff}(Q)$ calculated from Eq. **7a** using the dynamic model that parses *Taq* polymerase into two domains, the 5′ nuclease and the Klentaq domains. The blue line is the $D_{eff}(Q)$ calculated from Eq. **8** using the dynamic model that parses *Taq* polymerase into three domains, the 5′ nuclease, 3′–5′ exonuclease, and polymerase domains. (*B*) Static form factor $I(Q)$ of *Taq* polymerase measured by SAXS (●) and calculated from the crystal structure coordinates (PDB ID code 1TAQ.PDB) by a FORTRAN program (line). The scale of the *x* axis is the same as that shown in *A*. (*C*) Length distribution function $P(r)$ of *Taq* polymerase calculated from SAXS (○) and from the crystal structure coordinates (line).

from the crystal structure. The ensemble-averaged global structure of *Taq* polymerase in solution by SAXS is thus very close to the crystal structure. If there were distinct multiple structures, we would expect the SAXS results to be significantly different from the crystal structure. Thus, the oscillatory behavior of $D_{eff}(Q)$ measured by NSE shown in Fig. 4*A* must arise from the internal motions of *Taq* polymerase. In the following, we analyze the NSE results from *Taq* polymerase by using a normal mode framework and statistical mechanics to show how the oscillation in $D_{eff}(Q)$ can be explained by internal motion.

Normal Mode Analysis (NMA) Suggests That the Lowest Frequency Normal Modes of Internal Motions in *Taq* Polymerase Are Interdomain Motions. We have carried out NMA on *Taq* polymerase by using the program ELNEMO (34) to identify the type and direction of internal motion (35). In NMA, the first six modes of lowest frequency are the translational motion and rotational motion of the protein molecule as a whole. NMA suggests that the lowest frequency modes of internal motion, which are modes 7 and 8 (Fig. 1), are the *en bloc* relative motion between the 5′ nuclease and the Klentaq domains. The direction of motion of modes 7 and 8, shown in Fig. 1, is consistent with our previous structural study by small-angle neutron scattering that finds the 5′ nuclease domain to be in closer contact with the thumb subdomain when *Taq* polymerase binds to a structural specific overlap flap DNA (17). In higher normal modes, subdomain motions appear. Specifically, in normal modes 9 and 10, the relative motions of the 5′ nuclease, the 3′–5′ exonuclease, and the polymerase domains are apparent (see Fig. 1).

Thus, NMA predicts that the lowest frequency mode of internal motion in *Taq* polymerase involves the relative motions of two domains, the polymerase plus the 3′–5′ exonuclease domain (together called the Klentaq domain) and the 5′ nuclease domain, which are connected by a spring-like linker (see Fig. 5*B*). Higher normal modes display relative motion of three rigid domains, with the Klentaq domain split into its 3′–5′ exonuclease and polymerase components (see Fig. 5*C*).

NSE Can Determine the Domain Mobility Tensor That Defines the Degree of Dynamical Coupling Between Domains. The above analysis shows that a rigid-body analysis of *Taq* polymerase is inadequate and that the ensemble-averaged solution structure is very close to the crystal structure. We therefore generate a progression of models that systematically include internal normal modes by considering (*i*) the lowest frequency internal modes in which the 5′ nuclease and the Klentaq domains are treated as two oscillating lobes and (*ii*) the two lowest frequency modes that include the 5′ nuclease domain but in which the Klentaq domain is now further subdivided into its polymerase and 3′–5′ exonuclease domain components.

First, we treat the Klentaq domain and the 5′ nuclease domains as separate rigid objects whose coordinates are assumed to vary little from the crystal structures (see Fig. 5*B*). The time evolution of the coordinates can be described by the Langevin equation for the two domains at center-of-mass coordinates $\vec{r}_j$ ($j = 1,2$) that comprise the protein (36):

$$\frac{d}{dt}\vec{r}_j = \sum_k \overleftrightarrow{H}_{jk} \cdot \left[-\frac{\partial U\{r\}}{\partial \vec{r}_k} + \vec{f}_k(t) \right], \qquad [3]$$

where $\overleftrightarrow{H}_{j,k}$ is the domain mobility tensor and is defined by $\vec{V}_j = \Sigma_k \overleftrightarrow{H}_{jk} \cdot \vec{F}_k$ in terms of the velocities $\vec{V}_j$ and forces $\vec{F}_k$ for each domain. Here, U is the potential of mean force between the two domains and f is the usual random thermal force with ensemble averages
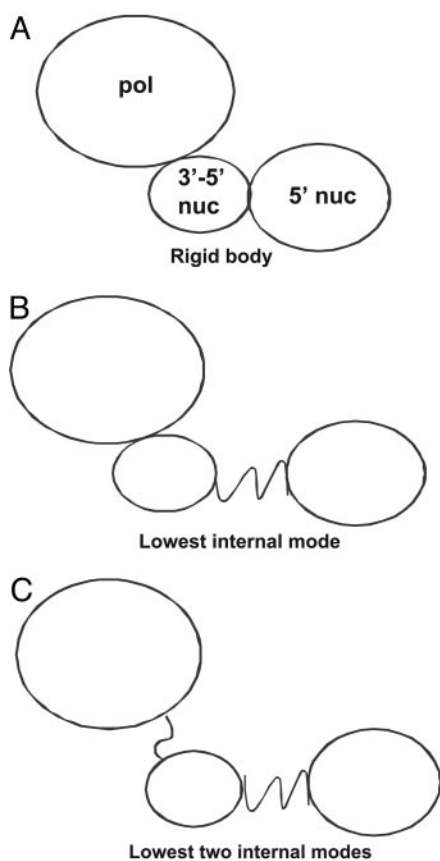
Fig. 5. Dynamic models of *Taq* polymerase. (*A*) Rigid-body model of *Taq* polymerase used in Eq. **2**. (*B*) Two-rigid-domain model connected by a spring-like linker calculated by Eq. **7a**. (*C*) Three-rigid-domain model connected by two spring-like linkers calculated by Eq. **8**.

$$\langle \vec{f}_j(t) \rangle = 0$$

$$\langle \vec{f}_j(t)\vec{f}_k(t') \rangle = 2(\bar{\bar{H}}^{-1})_{jk} k_B T \delta(t - t'),$$
[4]

where k_B is Boltzmann's constant and T is the temperature. Eq. **3** indicates that protein motion and thus its normal modes arise from a convolution of the static structural forces (U) and the dynamical and hydrodynamical effects (H).

The first cumulant (defined in *Methods*) of the dynamic form factor can be calculated, because effects that occur on different timescales can be separated (37–40). There are rapidly fluctuating "Brownian" forces due to collisions with solvent molecules, and, in addition, there are longer timescale forces on domains due to the influence of other domains. The first cumulant of $S(Q, t)/S(Q, 0)$ for the two-domain model is thus

$$D_{\text{eff}}(Q) = \frac{k_B T}{Q^2} \frac{\sum\limits_{j,k} b_j b_k \langle \vec{Q} \cdot \bar{\bar{H}}_{j,k} \cdot \vec{Q} \exp[i\vec{Q}\cdot(\vec{r}_j - \vec{r}_k)] \rangle}{\sum\limits_{j,k} b_j b_k \langle \exp[i\vec{Q}\cdot(\vec{r}_j - \vec{r}_k)] \rangle},$$
[5]

where $\{b_j\}$ are atomic neutron scattering lengths. The $D_{\text{eff}}(Q)$ of Eqs. **3**–**5** reveals the dynamic events that occur on the timescales of internal modes (9) that are much longer than the Brownian timescale τ_B (40).

It is important to point out that the formula Eq. **5** arises as the result of a delicate limiting process. A central feature of this process is the order in which two important limits are taken.

These limits are (*i*) the limit in which a stiff spring becomes perfectly rigid and (*ii*) the limit of zero time in the first cumulant of the effective diffusion constant. If the second limit is taken first, very fast underdamped modes can appear (32). In this case, it is no longer reasonable to neglect inertial modes, and the usual derivations of Eq. **5** are invalid. These difficulties can be avoided by taking limit (*i*) first (32). Thus, such relations are correct for perfectly rigid bodies (Eq. **2**) or for rigid bodies connected by soft spring linkers (Eq. **5**), as we consider in this study. The existence of underdamped motion requires that the spring constant for a linker connecting domains of mass m and friction constant ζ be $>\zeta^2/4m$ (9); explicit calculations as well as measurements (23) indicate that proteins are well within the overdamped soft spring regime.

Eqs. **2**, **4**, and **5** explicitly show that, given the structural coordinates of a protein, the NSE experiment essentially tests models of the domain mobility tensor $\bar{\bar{H}}_{j,k}$, which defines the velocity $\vec{v}_j$ of domain j given the force $\vec{F}_k$ applied to domain k. We construct the simplest possible model of a domain mobility tensor for internal motion

$$\bar{\bar{H}}_{j,k} = \zeta_j^{-1}\delta_{j,k}\bar{\bar{I}}$$
[6]

with friction constants ζ_j, $j = 1, 2$ appropriate for each domain and evaluate $D_{\text{eff}}(Q)$ using Eq. **5** for the case in which *Taq* polymerase is separated into two domains, a 5′ nuclease domain ($j = 1$) and a Klentaq domain ($j = 2$). The $D_{\text{eff}}(Q)$ for the two-domain model (see Fig. 5*B*) is then

$$D_{\text{eff}}(Q) = \frac{D_1 S_1(Q) + D_2 S_2(Q)}{S_{Taq}(Q)},$$
[7a]

where $D_j = (k_B T)/\zeta_j$ with $D_1 = D_{5'\text{-nuc}}$ and $D_2 = D_{\text{Klentaq}}$, and

$$S_j(Q) = \sum_{m,n \in j} b_m b_n \frac{\sin[Q|r_m - r_n|]}{Q|r_m - r_n|}$$
[7b]

$$S_{Taq}(Q) = \sum_{m,n=1}^{N_1 + N_2} b_m b_n \frac{\sin[Q|r_m - r_n|]}{Q|r_m - r_n|}$$
[7c]

are the rotationally averaged static form factors, which can be approximated by the crystal structure coordinates as we show by SAXS (see *Unusual Internal Dynamic Behavior in* Taq *Polymerase Revealed by NSE*) and previous small-angle neutron scattering studies (17). In Eq. **7b**, the sum is taken over the N_j atoms in domain j, and N_1 and N_2 are the number of atoms in domain 1 and domain 2, respectively. The cross-term 1–2 in the numerator of Eq. **7a** disappears because the mobility tensor is diagonal. Subtleties in using Eq. **7** arising when rigid constraints are applied (41–44) are avoided by explicitly separating the center-of-mass coordinate of each domain before performing the ensemble average and then subsequently folding in domain form factors. Eq. **7** was also verified by explicit calculation using Eq. **2** with U taken as a harmonic oscillator potential. As per Eq. **7**, the first cumulant is explicitly independent of the interdomain spring constant.

The calculated $D_{\text{eff}}(Q)$ using Eq. **7a**, shown in Fig. 4*A*, also has peaks and dips in the intermediate Q values as the NSE-measured $D_{\text{eff}}(Q)$. When using Eq. **7a** to calculate the curves shown in Fig. 4*A*, we find that the friction constants ζ_1 and ζ_2 of both domains in *Taq* polymerase increase by a factor of ≈2 compared with those of the separated individual domains as calculated by the Kirkwood–Riseman formula (45). As the domains are in close proximity, the friction constant for each domain is increased because of the fluid displaced between them by their motion. Quantitatively similar phenomena have been found when two circular disks or two spheres

approach one another in viscous media or when a sphere approaches a wall (9, 46–48).

We then extend Eq. **7a** to the case of a three-domain model (see Fig. 5C). In this model, the Klentaq domain is subdivided into the $3'–5'$ exonuclease and polymerase domains. We then repeat the analysis of Eqs. **7** to show

$$D_{\mathrm{eff}}(Q)$$

$$= \frac{D_{5'\text{-nuc}}S_{5'\text{-nuc}}(Q) + D_{3'\text{-}5'\text{nuc}}S_{3'\text{-}5'\text{nuc}}(Q) + D_{\mathrm{pol}}S_{\mathrm{pol}}(Q)}{S_{Taq}(Q)}.$$

[8]

The result calculated by Eq. **8** appears in Fig. 4A and demonstrates that the systematic inclusion of higher normal modes consistently improves the agreement with the NSE experiment. Thus, our mobility tensor analysis shows that NSE data reveal coupled correlated domain motion within *Taq* polymerase. Moreover, we show that the internal motion can be systematically analyzed by reducing the data within a normal mode framework.

The rms amplitude $\langle x^2 \rangle^{1/2}$ and the spring constant of interdomain motion can be estimated from the equipartition theorem, which states

$$\langle x^2 \rangle = \frac{k_{\mathrm{B}}T}{k} = \left(\frac{k_{\mathrm{B}}T}{\zeta}\right)\left(\frac{\zeta}{k}\right) = D\tau,$$

[9]

where k is the spring constant, k_{B} is Boltzmann's constant, D is the Stokes–Einstein diffusion constant, τ is the relaxation time that can be estimated from the NSE results, and T is the temperature. Thus, for relaxation times of the order of 10 ns, the estimated amplitude $\langle x^2 \rangle^{1/2}$ of the normal mode is ≈ 1–10 Å. For $\langle x^2 \rangle^{1/2} = 7$ Å, the spring constant k for the linker region is $\approx 8.5 \times 10^{-3}$ N/m. This value is less than one-third of the spring constant of myoglobin (23) but ≈ 5.6 times larger than the reported spring constant of cross-linked polystyrene (49).

In summary, protein conformational changes are typically initiated through an ensemble of states that interconvert on picosecond to nanosecond timescales (50). These small-amplitude conformational changes (Eyring dynamics) can eventually encourage thermally activated (Kramers kinetics) events that lead to large-scale conformational changes on the nanosecond to microsecond timescale (9). Our NSE results have revealed coupled motion between protein domains that are separated by 70 Å. On the nanosecond timescales probed by NSE, this coupled domain motion is an overdamped, creeping motion rather than the harmonic oscillation expected for inertial motion (9, 51). We show how NSE can determine the domain mobility tensor of a protein and thus characterize dynamic interdomain coupling. The mobility tensor defines the velocity response of a given domain to a force applied to it or to another domain, much as the sails determine the velocity (direction and magnitude) of a sailboat's travel when a given wind force is applied. NSE thus provides unique dynamic information about a protein that is functionally important and inaccessible by other methods.

1. Gai, D., Zhao, R., Li, D., Finkielstein, C. V. & Chen, X. S. (2004) *Cell* **119**, 47–60.
2. Young, M. A., Gonfloni, S., Superti-Furga, G., Roux, B. & Kuriyan, J. (2001) *Cell* **105**, 115–126.
3. Graceffa, P. & Dominguez, R. (2003) *J. Biol. Chem.* **278**, 34172–34180.
4. Bose-Basu, B., DeRose, E. F., Kirby, T. W., Mueller, G. A., Beard, W. A., Wilson, S. H. & London, R. E. (2004) *Biochemistry* **43**, 8911–8922.
5. Joyce, C. M. & Benkovic, S. J. (2004) *Biochemistry* **43**, 14317–14324.
6. Li, Y., Korolev, S. & Waksman, G. (1998) *EMBO J.* **17**, 7514–7525.
7. Gerstein, M. & Krebs, W. (1998) *Nucleic Acids Res.* **26**, 4280–4290.
8. Berg, O. G. & von Hippel, P. H. (1985) *Annu. Rev. Biophys. Biophys. Chem.* **14**, 131–160.
9. Howard, J. (2001) *Mechanics of Motor Proteins and the Cytoskeleton* (Sinauer, Sunderland, MA).
10. Gelles, J. & Landick, R. (1998) *Cell* **93**, 13–16.
11. Lyamichev, V., Brow, M. A. & Dahlberg, J. E. (1993) *Science* **260**, 778–783.
12. Kaiser, M. W., Lyamicheva, N., Ma, W., Miller, C., Neri, B., Fors, L. & Lyamichev, V. I. (1999) *J. Biol. Chem.* **274**, 21387–21394.
13. Xu, Y., Grindley, N. D. & Joyce, C. M. (2000) *J. Biol. Chem.* **275**, 20949–20955.
14. Kornberg, A. & Baker, T. A. (1992) *DNA Replication* (Freeman, San Francisco).
15. Kim, Y., Eom, S. H., Wang, J., Lee, D. S., Suh, S. W. & Steitz, T. A. (1995) *Nature* **376**, 612–616.
16. Joubert, A. M., Byrd, A. S. & LiCata, V. J. (2003) *J. Biol. Chem.* **278**, 25341–25347.
17. Ho, D. L., Byrnes, W. M., Ma, W. P., Shi, Y., Callaway, D. J. & Bu, Z. (2004) *J. Biol. Chem.* **279**, 39146–39154.
18. Steitz, T. A. (1999) *J. Biol. Chem.* **274**, 17395–17398.
19. Ma, W. P., Kaiser, M. W., Lyamicheva, N., Schaefer, J. J., Allawi, H. T., Takova, T., Neri, B. P. & Lyamichev, V. I. (2000) *J. Biol. Chem.* **275**, 24693–24700.
20. Ewen, B. & Richter, D. (1997) *Adv. Polym. Sci.* **134**, 1–129.
21. Mezei, F., Pappas, C. & Gutberlet, T. (2003) *Neutron Spin Echo Spectroscopy: Basics, Trends, and Applications* (Springer, Berlin).
22. Perez, J., Zanotti, J.-M. & Durand, D. (1999) *Biophys. J.* **77**, 454–469.
23. Zaccai, G. (2000) *Science* **288**, 1604–1607.
24. Gabel, F., Bicout, D., Lehnert, U., Tehei, M., Weik, M. & Zaccai, G. (2002) *Q. Rev. Biophys.* **35**, 327–367.
25. Tehei, M., Franzetti, B., Madern, D., Ginzburg, M., Ginzburg, B. Z., Giudici-Orticoni, M. T., Bruschi, M. & Zaccai, G. (2004) *EMBO Rep.* **5**, 66–70.
26. Bu, Z., Cook, J. & Callaway, D. J. (2001) *J. Mol. Biol.* **312**, 865–873.
27. Monkenbusch, M., Schatzler, R. & Richter, D. (1997) *Nucl. Instrum. Methods Phys. Res. Sect. A* **399**, 301–323.
28. Bu, Z., Perlo, A., Johnson, G. E., Olack, G., Engelman, D. M. & Wyckoff, H. W. (1998) *J. Appl. Crystallogr.* **31**, 533–543.
29. Glatter, O. & Kratky, O. (1982) *Small Angle X-Ray Scattering* (Academic, New York).
30. Carrasco, B. & Garcia de la Torre, J. (1999) *Biophys. J.* **76**, 3044–3057.
31. Garcia de la Torre, J., Huertas, M. L. & Carrasco, B. (2000) *Biophys. J.* **78**, 719–730.
32. Song, L., Kim, U. S., Wilcoxon, J. & Schurr, J. M. (1991) *Biopolymers* **31**, 547–567.
33. Gebe, J. A. & Schurr, J. M. (1993) *Biopolymers* **33**, 1757–1764.
34. Suhre, K. & Sanejouand, Y. H. (2004) *Nucleic Acids Res.* **32**, W610–W614.
35. Krebs, W. G., Alexandrov, V., Wilson, C. A., Echols, N., Yu, H. & Gerstein, M. (2002) *Proteins* **48**, 682–695.
36. Lax, M. (1960) *Rev. Mod. Phys.* **32**, 25–64.
37. Pusey, P. N. (1975) *J. Phys. A Math. Gen.* **8**, 1433–1440.
38. Ackerson, B. J. (1976) *J. Chem. Phys.* **64**, 242–246.
39. Akcasu, Z. & Gurol, H. (1976) *J. Polym. Sci. B Polym. Phys.* **14**, 1–10.
40. Pusey, P. N. & Tough, R. J. A. (1982) *J. Phys. A Math. Gen.* **15**, 1291–1308.
41. Akcasu, A. Z., Benmouna, M. & Han, C. C. (1980) *Polymer* **21**, 866–890.
42. Han, C. C. (1996) *J. Polym. Sci. B Polym. Phys.* **34**, 2113–2115.
43. Stockmayer, W. H. & Burchard, W. (1979) *J. Chem. Phys.* **70**, 3138–3139.
44. Fixman, M. (1988) *J. Chem. Phys.* **89**, 2442–2462.
45. Kirkwood, J. G. & Riseman, J. (1948) *J. Chem. Phys.* **16**, 565–573.
46. Landau, L. D. & Lifshitz, E. M. (1975) *Fluid Mechanics* (Pergamon, New York).
47. Happel, J., Brenner, H. & Moreau, R. J. (1983) *Low Reynolds Number Hydrodynamics: With Special Applications to Particulate Media (Mechanics of Fluids and Tranport Processes)* (Kluwer, Boston).
48. Stimson, M. & Jeffery, G. B. (1926) *Proc. R. Soc. London Ser. A* **111**, 110.
49. Jensenius, H. & Zocchi, G. (1997) *Phys. Rev. Lett.* **79**, 5030–5033.
50. Lindorff-Larsen, K., Best, R. B., Depristo, M. A., Dobson, C. M. & Vendruscolo, M. (2005) *Nature* **433**, 128–132.
51. Miyashita, O., Onuchic, J. N. & Wolynes, P. G. (2003) *Proc. Natl. Acad. Sci. USA* **100**, 12570–12575.

BIOPHYSICS